Heliyon 7 (2021) e08064

Contents lists available at ScienceDirect

Heliyon

journal homepage: www.cell.com/heliyon

Research article

Electric vehicles fire protection during charge operation through Vanadium-air flow battery technology

L. Barelli [a,*], G. Bidini [a], P.A. Ottaviano [a], D. Pelosi [a], M. Perla [a], L. Trombetti [a], F. Gallorini [b], M. Serangeli [b]

[a] Department of Engineering, University of Perugia, Via G. Duranti 93, Perugia 06125, Italy
[b] VGA srl, Via Ugo Foscolo, 1, Deruta 06053, Italy

ARTICLE INFO

Keywords:
Electric vehicles
Li-ion batteries
Vanadium-air flow batteries
Safety
Vehicle-to-grid

ABSTRACT

During the last decade, electric vehicles had a remarkable diffusion caused by Li-ion batteries lowered prices and improved performances. Meanwhile, incidents involving fire were reported for electric vehicles during charge operation or simple parking. The potential drawbacks of this technology could play a role on safety in the next years, especially for household or underground charge. This paper presents the development of a novel system concept based on a Vanadium-air flow battery, applied to provide charge and fire safety of electric vehicles through oxygen reduction in a sealed box. When the vehicle is parked inside the box and the passengers are outside of it, a nitrogen injection is operated to reduce the fire risk quickly, during the subsequent vehicle charge operation the oxygen is consumed from the box atmosphere by the cathode of the Vanadium-air battery that supplies energy, then the nitrogen reserve is restored consuming oxygen from the external ambient and the energy output can be supplied to smart grids. The system is mainly composed by the Vanadium-air flow battery, the protection box and the nitrogen reserve, it is sized relatively to the most diffused road and commercial electric vehicles for different values of on-board battery capacity and charge power Moreover, it can be integrated into vehicle-to-grid energy systems improving intersectoral flexibility.

1. Introduction

Li-ion batteries are the most used in electric vehicles (EV), this established technology exhibits safety issues related to *thermal runaway*, a phenomenon resulting from cell abuse involving fire and explosion consequences. A series of exothermic reactions leads to cell self-overheating and flammable gas emission that can propagate from the cell level to a whole battery pack with consequent fire or explosion [1]. Different root causes can trigger this effect, such as cell mechanical abuse, thermal abuse or electrical abuse [2]. It evolves with a first phase of self-heat generation, that is considered consistent with the decomposition of the solid electrolyte interface [3], then a second phase is characterized by fast temperature rise to the maximum temperature [4]. Thermal runaway can be detected through a typical voltage drop 15–40 s before the overheating onset [5]. Despite this any automatic system shut down operation is not effective against thermal runaway. The measured activation temperatures are 104÷144 °C [6] for most of the cell chemistries and 246 °C for LFP cells [7].

Self-ignited EV fires during charge were reported during the last years, with causes such as external short circuit, previous cell damage, charger fault [8]. Cases of long-duration fires were reported, for small EV with low capacity batteries [9], luxury cars [10, 11] and vans [12] involving fire and smoke damages to the nearby buildings [9, 10]. Potential damages are higher during charge, batteries with high state of charge have an increased heat rate release in case of fire; moreover, charge operation could be performed in a residential environment during the night with no control.

EVs are not equipped with automated fire suppression systems; in case of fire the extinguishing function must be operated by an external system. During fire tests on electric vehicle batteries, water shows high effectiveness in the cooling effect [13, 14, 15]. Conversely, as estimated in an EV test, to complete firefighting procedures is necessary a huge amount of water, up to 10 m^3 [15].

It's important to underline as also battery shells and cases curtail the action of water, so an automated suppression system can only be effective after the fire has spread to the car body.

* Corresponding author.
E-mail address: linda.barelli@unipg.it (L. Barelli).

https://doi.org/10.1016/j.heliyon.2021.e08064
Received 21 April 2021; Received in revised form 27 April 2021; Accepted 21 September 2021

This work describes the concept of an EV box protected through an oxygen reduction system (ORS) based on a vanadium air flow battery (VAB). Such system could be able to create a low-oxygen atmosphere, avoiding fire spreading and subsequent damages, providing at the same time the EV charge. To this regard, it is highlighted as VAB utilization contributes also to the mitigation of EV integration to the grid. Hence, the VAB is used as a fire protection device and power source as well as a battery energy storage system (BESS).

2. EV models and categories

Global sales of EV reached 2.1 million in 2019 and an overall stock of 7.2 million; 2.1 million in Europe, where the market growth average from 2017 is 39% per year [16]. Sector outlook shows a possible growth of the global EV fleet, reaching 116 million in 2030 [17], EU sales per year of around 6.7 million units in 2030 [18] and EU vehicle production of 2.5 million units in 2025 [19]. To perform charging system sizing, features of most diffused EV models were investigated. Historical data of registered EVs at Italian Motor Vehicle Department from 2013 to 2019 [20] were analyzed, a classification of EV models can be reassumed in Table 1, where the reported number of vehicles must be intended as above the indicated value.

The EV models were divided by battery capacity in two categories, low and high capacity, below and above 35 kWh respectively. Discontinued models were not included in this evaluation, data are summarized in Table 2.

Electric commercial vehicles were also evaluated, no data of registered vehicles by model are available, hence, few models were taken as reference. Features are reassumed in Table 3.

Four categories were defined, classified by utilization, road or commercial, and battery capacity, low and high. Box volume was calculated taking as reference the maximum vehicle dimensions per category. To calculate volume height, 0.2 m were added to the real maximum vehicle dimension (2 m is set as the minimum protected volume height), volume length was calculated adding 0.4 m and width adding 0.8 m respectively. Protected box dimensions are reassumed in Table 4.

3. Box protection strategy through VAB operation

ORS concept aims to create a protected area to prevent ignition and fire development; system design is regulated by EN 16750 standard [21]. The oxygen level to be reached is called Limiting Oxygen Concentration (LOC) or Minimum Oxygen Concentration (MOC). For most fuels, an oxygen concentration of 10% can prevent ignition, lower values are expected for carbon disulfide (5%), carbon monoxide (5.5%), hydrogen (5%), hydrogen sulfide (7.5%) and aluminum (5%) [22]. The thermal runaway phenomenon is characterized by flammable gas emission, mixture composition for typical cell chemistries is reported in Table 5.

Table 1. Most diffused EV models in Italy.

Manufacturer	Model	Items
Nissan	Leaf	4725
Renault	Zoe	4423
Smart	Fortwo	4118
Tesla	Model 3	2206
Tesla	Model S	1211
BMW	I3	1158
Smart	Forfour	813
Tesla	Model X	689
Citroen	C0	559
Hyundai	Kona	470
Jaguar	I-Pace	299

Table 2. EV battery capacity classification.

Low-capacity Road vehicles (LCR)		
Manufacturer	Model	Capacity [kWh]
Smart	ForTwo	17.6
Smart	ForFour	17.6
Renault	Zoe	22 (41 optional; 52 latest version)
Nissan	Leaf	24 (30 optional)
BMW	i3	33 (42 latest version)
High-capacity Road vehicles (HCR)		
Manufacturer	Model	Capacity [kWh]
Hyundai	Kona EV	39.2 (64 optional)
Tesla	Model 3	50 (75 optional)
Tesla	Model S	60 (75 optional)
Tesla	Model X	60 (70÷100 optional)
Jaguar	I-Pace	90

Table 3. Electric commercial vehicle battery capacity classification.

Low-capacity commercial vehicles (LCC)		
Manufacturer	Model	Capacity [kWh]
Citroen	C0 – van	14.5
Citroen	Berlingo van	22.5
Peugeot	Partner electric	22.5
Renault	Kangoo z.e.	33
High-capacity commercial vehicles (HCC)		
Manufacturer	Model	Capacity [kWh]
Saic	EV-80	53
Nissan	e-NV 200	40
Iveco	Daily electric	60

Table 4. Protected volume dimensions.

	Height [m]	Length [m]	Width [m]	Gross box Volume [m^3]
LCR	2	4.9	2.9	28.42
HCR	2	5.5	3	33
LCC	2.7	6.6	3.3	58.81
HCC	2.9	6.1	2.8	49.53

Table 5. Thermal runaway vent gas mixture compositions [23].

	LCO/NMC	NMC	LFP
H_2 [%]	30	30.8	30.9
CO_2 [%]	24.9	41.2	53
CO [%]	27.6	13	4.8
CH_4 [%]	8.6	6.8	4.1
C_2H_4 [%]	7.7	8.2	6.8
C_2H_6 [%]	1.2	-	0.4

The LOC values for Li-ion thermal runaway vent gas mixtures are calculated through a method proposed by Zlochower et al. [24], expressed by Eq. (1):

$$LOC = \sum X_i r_i \Big/ \sum X_i r_i / (LOC)_i \quad (1)$$

Where X_i represents the combustible component molar fraction for the given mixture, r_i is the oxygen to fuel ratio, and $(LOC)_i$ is the theoretical value for component i. LOC values for the mixture components are reported in Table 6, while the calculated LOC for vent gas mixtures is reassumed in Table 7.

Therefore, as suggested in standard EN 16750, O_2 maximum concentration is set at 6.7% with a safety margin (−0.75%). VAB could be used as a nitrogen generator in an ORS: when the cathode is connected to the environment to be protected O_2 is consumed during discharge (d), as described by Eqs. (2), (3), and (4).

$$ANODE: \ 4V^{2+} \rightleftarrows_{(c)}^{(d)} 4V^{3+} + 4e^{-} \quad (2)$$

$$CATHODE: \ O_2 + 4e^{-} + 4H^{+} \rightleftarrows_{(c)}^{(d)} 2H_2O \quad (3)$$

$$CELL: \ 4V^{2+} + O_2 + 4H^{+} \rightleftarrows_{(c)}^{(d)} 4V^{3+} + 2H_2O \quad (4)$$

Oxygen consumption from the VAB cathode during discharge (vehicle battery charge), depends on VAB cell current in A, as calculated by Eq. (5).

$$I = Q_{O_2} \cdot F \cdot n_{e^-} \ [A] \quad (5)$$

where:

- Q_{O_2} [mol s^{-1}] represents the oxygen flow,
- F is the Faraday constant (96,485 C mol^{-1})
- n_{e^-} is the number of electrons per mol (equal to 4 according to Eq. (3)) per consumed oxygen mole at the cathode.

The box protection strategy is based on the following procedure:

1. Once the vehicle is inside the protected volume and is connected to the charging device, a first injection of N_2 is provided through a specific channel. During this phase the O_2 concentration is lowered to 11% by purging, through a channel for air discharge. For this purpose, the box main door is closed and airtight, system must be activated through an external control in order to avoid the presence of people inside the box.
2. During the EV charge the O_2 concentration is further lowered down to 6.7% in order to avoid gas combustion and fire in case of vehicle battery thermal runaway. The second phase of the inertization procedure is based on VAB operation, consuming O_2 from the protected volume environment, through internal air recirculation at the cathode section, channels described at point 1 are closed.
3. The N_2 to be injected during the phase described at point 1 is produced from external air through the VAB operation and stored in a cylinder pack. During this third phase, the EV charge is completed. If the amount of the produced N_2 is not sufficient to provide the injection described at point 1, the VAB operation will continue supplying energy to the grid/utility.

3.1. Technical and economic feasibility

A single cell VAB consists of two half-cells separated by a commercial ionomeric membrane (e.g. NafionTM 211 purchased from Ion Power, GmbH) and synthetic fluoropolymer elastomer seals. As evident in the diagram below (see Figure 1), a polycarbonate block is placed with mechanical connections, electrolyte collectors, current collector and electrode connections on each side. The current collectors are made of a graphite polypropylene composite bipolar plate and the electrodes are graphite felts. On the cathode side a carbon cloth gas diffusion layer with Pt catalyst is placed between graphite felt and the current collector.

Table 6. LOC values [22].

GAS	LOC $(\%)_{vol}$
H_2	5
CO	5.5
CH_4	12
C_2H_4	10
C_2H_6	11

Table 7. Vent gas calculated LOC.

Vent Gas Mixture	LCO/NMC	NMC	LFP
LOC_{mix} $(\%)_{vol}$	7.60	7.65	7.5

VAB is a technology at early stage compared to other battery technologies. Indeed, nowadays the challenges of such batteries are related to long-term stability, high concentration of Vanadium species in the anolyte, efficient water management at the cathode and higher current and energy densities [26]. Hence, the research is currently endeavoring to find a low cost, efficient and stable catalyst both for oxygen reduction reaction (ORR) and oxygen evolution reaction (OER) in order to increase the slow kinetics of oxygen involved reactions [27]. Since VAB consumes oxygen during discharge as already detailed by Eqs. (2), (3), and (4), it is characterized by a relevant added value in term of fire safety when employed to charge an electric vehicle in a sealed box.

Nowadays, considering the ever-growing focus on electric mobility, VAB technology can turn out to be a fundamental application also considering the lack of early warning systems against Li-ions battery thermal runaway. Currently, emergency alarms are activated when a fault is detected, around 5 min before dangerous conditions are achieved, hence the current systems could be considered not sufficient for protection during charge [28].

As explained above, the fire protection concept of an ORS system is based on lowering the oxygen levels before the fire starts, then nitrogen generators can be considered more convenient if compared with N_2 purchase.

It is important to notice that the consumed N_2 to reach an oxygen concentration of 11% ranges between 14.8 and 25.8 m^3 (at 1 atm and 273.15 K) as expressed in moles in Table 12 after the calculations described in section 4. According to current estimations the VAB cost may be in the range of 15–40 k€, as reported in the literature [26] for the sizes evaluated in this work, 10 kW and 18 kW as detailed in section 4 (capacities from 24 to 90 kWh, see Table 13).

Starting from these preliminary evaluations it is possible to roughly estimate the minimum VAB lifetime which has to be targeted in the future technology development to make this solution economical if compared to nitrogen purchase.

In particular, considering an average cost of 260 € to buy a V16 N_2 bulk pack (16 cylinders of 50 L each) @200 bar, about 11 and 6 EV charges are possible considering a N_2 consumption per charge of 14.8 and 25.8 m^3 (at 1 atm and 273.15 K) respectively. In the following an average value of 8.5 EV charges is considered with a frequency of 1

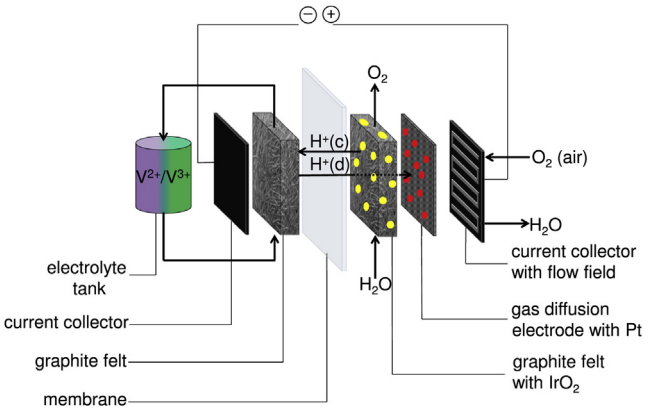

Figure 1. Single cell VAB scheme [25].

charge per day, thus 260 € can be the operation cost of the ORS system for 8.5 days.

With these assumptions, considering an average VAB cost of 27.500€, it is possible to purchase about 110 V16 N_2 bulk pack with the same expense. Consequently, VAB has to achieve a lifetime of at least 2.5 years to become competitive. Such a rough estimation doesn't consider the technical and economic advantages obtained in terms of optimization of the power profile absorbed from the grid with respect to the EV charging power profile. Moreover, renewable power available at the user can be exploited to this aim thanks to the adoption of the VAB as a stationary storage device.

3.2. Preliminary experimental activity

This section describes a preliminary experimental activity that was carried out to assess cell performance in terms of voltage output under relevant current density and operating conditions [29, 30]. The obtained data are used as input for the system concept development, further activities are necessary in order to perform a validation at full-scale levels, including vehicles. The tested VAB cell, with an active area of 12 cm^2, consisted of a sandwich of several components. The VAB cell was composed by two half-cells divided by two membranes. An intermediate chamber was used to avoid the diffusion of divalent vanadium ions (V^{2+}) to the Pt-catalyst, as indicated in [30]. It consisted of a flow-through polypropylene frame, realized by means of 3D printing, in which an aqueous solution with 4.2M of sulphuric acid flowed through by a peristaltic pump. The anodic half-cell was composed of a graphite plate and a Teflon frame including the carbon felt electrode (Sigracell GFD 4.6 EA, SGL carbon GmbH). Santoprene™ gaskets were placed in between for sealing. A Nafion® 211 membrane separated the anodic half-cell from the intermediate chamber. The anolyte solution was composed by 1.6M vanadium electrolyte with 4.2M sulphuric acid concentration stabilized with 0.05M phosphoric acid (Oxkem, UK) and it is circulated by a peristaltic pump through the anodic half-cell. Cathodic half-cell was comprised of a graphite plate, a Teflon flow frame, a gas diffusion layer (Sigracet 39 BB, SGL carbon GmbH), a Santoprene™ gasket and a catalyst coated membrane (CCM PEFC 1.0 mg Pt cm^{-2} on Nafion® 212, balticFuelCells GmbH). An air flow was fluxed within the cathode. Moreover, aluminum plates were employed to compress the inner components by means of an 8 screws system and copper plates were used as current collectors. A preliminary test was carried out by means of BioLogic SP-240 equipment. VAB test rig is shown in Figure 2.

Experimental activity was conducted discharging the VAB at a constant current density of 20 mA cm^{-2} at ambient temperature (293 K), according to [29, 30]. Discharge voltage was measured by BioLogic SP-240, the resulting voltage evolution is illustrated in Figure 3. The mean value deduced from experimental test (i.e. 0.95 V) was used as input for VAB stack sizing.

3.3. Flow calculations

Oxygen concentration is reduced in the protected volume therefore, pressure is also reduced. A further flow of external air is treated by the VAB and injected to maintain an overpressure of 25 Pa, in order to avoid the entry of external air (and therefore O_2) into the protected environment.

The number of oxygen moles ($n_{O_{2,V}}$) to be consumed to reach the target concentration can be calculated according to Eq. (6).

$$n_{O_{2,V}} = \frac{P_1 V}{RT} \cdot \left(1 - \frac{100 - X_{O_{2,1}}}{100 - X_{O_{2,t}}}\right) [mol] \quad (6)$$

Where:

- P_1 [Pa] is the internal pressure set to 101,350 Pa,
- V [m^3] is the gross box volume,

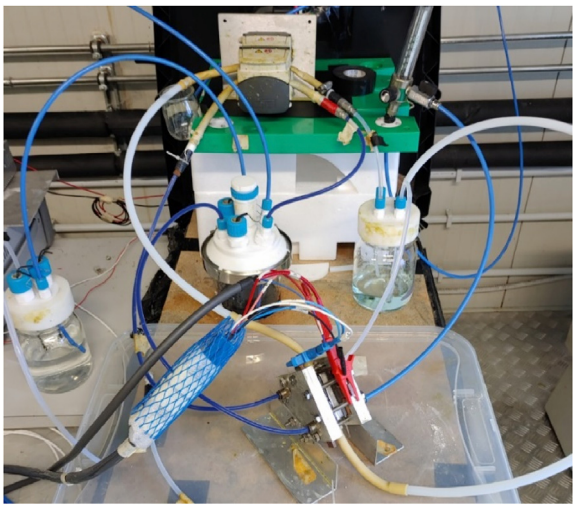

Figure 2. Test rig of the VAB cell.

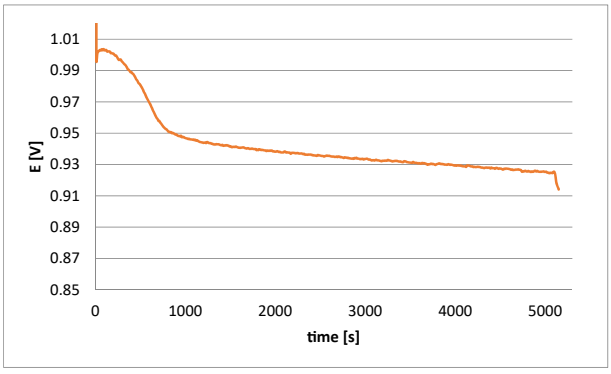

Figure 3. Measured voltage trend for the VAB cell.

- T [K] is the internal temperature,
- R [J mol^{-1} K^{-1}] is the ideal gas constant equal to 8,314,
- $X_{O_{2,1}}$ is the oxygen concentration in the protected volume after the N_2 injection, set to 11%,
- $X_{O_{2,t}}$ is the target oxygen concentration set to 6.7 %.

It is highlighted as the 11% $X_{O_{2,1}}$ value was determined also considering the CFD simulation outcomes of the N_2 injection process in the EV box. The CFD investigation was aimed also to the setting of suitable area and positioning of both N_2 inlet and the discharge channel. Some details are provided in section 3.3.

In order to keep the box pressure at the desired level, a supplementary injection of oxygen reduced air must be supplied, the corresponding number of oxygen moles ($n_{O_{2,add}}$) to be consumed are determined according to Eq. (7).

$$n_{O_{2,add}} = n_{O_{2,V}} \cdot \left(\frac{100 - X_{O_{2,t}}}{100 - X_{O_{2,std}}} - 1\right) [mol] \quad (7)$$

Where $X_{O_{2,std}}$ is the standard oxygen concentration set at 20.9%.

VAB features, as determined in the experimental test taking into account [30], are:

- current density of 20 mA cm^{-2};
- cell rated voltage of 0.95 V at 20 mA cm^{-2}.

Total consumed O_2 flow ($Q_{O_{2,VAB}}$) is calculated by Eq. (8).

$$Q_{O_{2,VAB}} = \left(n_{O_{2,V}} + n_{O_{2,add}}\right) \cdot \left(\frac{W}{E \cdot \leq F \cdot n_{e^-}}\right) \left[mol\, s^{-1}\right] \quad (8)$$

where W is battery power expressed in W, E is the rated single cell voltage set at 0.95 V, F is the Faraday constant (96,485 C mol^{-1}) and n_{e^-} is the number of electron moles (equal to 4 according to Eq. (3)). The O_2 consumed flow from the protected volume ($Q_{O_{2,V}}$) can be calculated by Eq. (9).

$$Q_{O_{2,V}} = Q_{O_{2,VAB}} \cdot \left(\frac{100 - X_{O_{2,std}}}{100 - X_{O_{2,t}}}\right) \left[mol\, s^{-1}\right] \quad (9)$$

The amount of N_2 to be injected in the protected volume during the phase described at point 1 of the protection strategy can be calculated by Eq. (10), representative of substitution purging.

$$n_{N_{2,inj}} = \frac{P_1 V}{RT} \cdot \left(\frac{X_{O_{2,std}} - X_{O_{2,1}}}{X_{O_{2,std}}}\right) \cdot N \left[mol\right] \quad (10)$$

Where N is a safety parameter that considers N_2 losses at the air discharge channel during the injection phase, equal to 1.2. Specifically, it is defined as the real injected N_2 amount, necessary to achieve the $X_{O_{2,1}}$ goal, over the theoretical quantity. The latter is deduced from Eq. (10) considering a unitary safety parameter.

A value of 1.2 was determined for the N parameter based on the assessment of N_2 losses through CFD investigations described in the following section 3.3.

3.4. CFD simulation of the N_2 injection process in the vehicle box

An Ansys Fluent CFD model of the N_2 injection process in the EV box was developed, including the EV shape. The box configuration was sized according to the dimensions reported in Table 4 for LCR vehicles. Simulations were performed setting a speed of 2.17 m/s for the N_2 flow at the inlet and considering an injection time of 60 s.

Moreover, suitable areas and positioning of the N_2 inlet and discharge channels were designed by monitoring the N_2 delivered in the atmosphere, aiming to reduce N_2 losses during the injection (Figure 4). N_2 losses were determined by processing the trends of both total mass flow rate and related N_2 molar fraction at the discharge channel during all the process. The final configuration is characterized by an upper N_2 inlet and a lower discharge channel on the same side of the box (Figure 4),

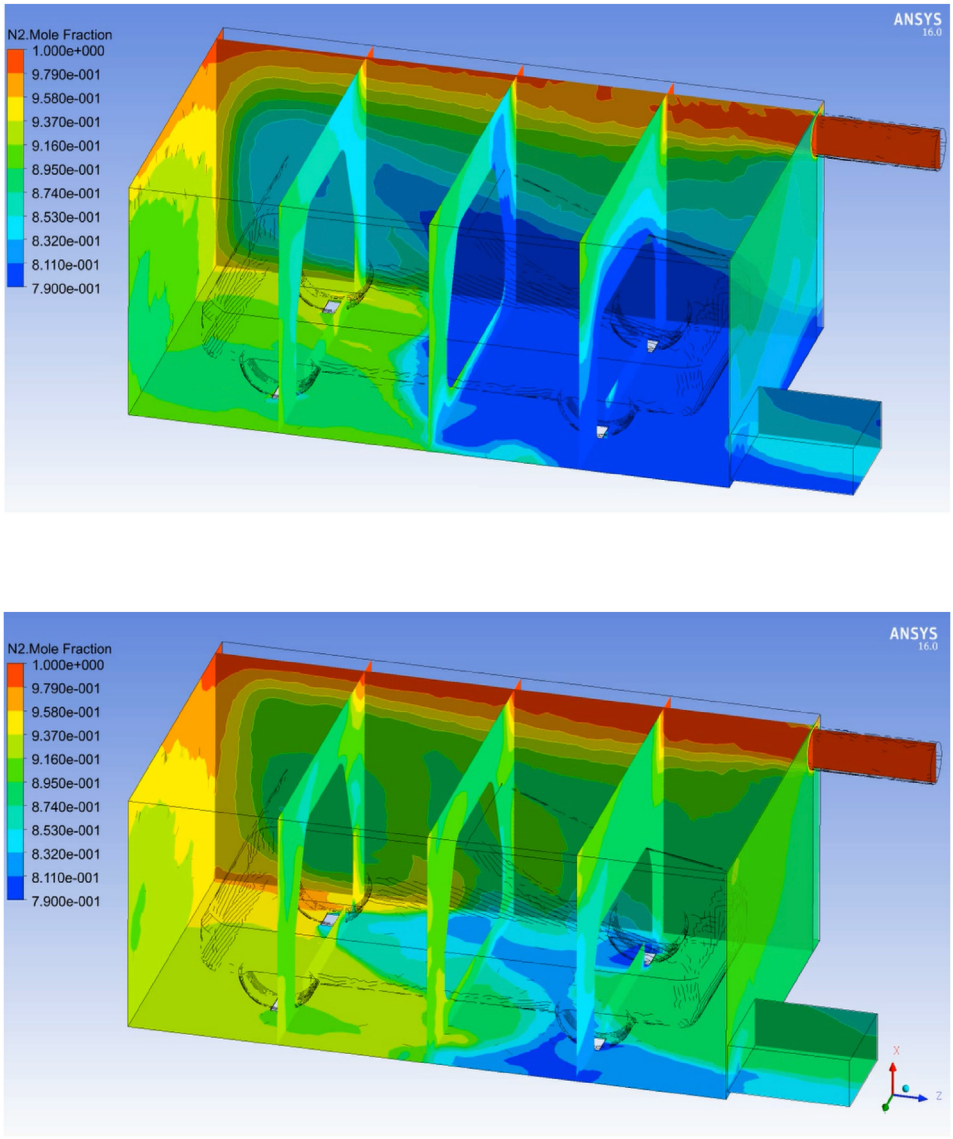

Figure 4. Box N_2 injection flow simulation at t = 30s (upper picture) and t = 60s (lower picture).

Table 8. Vehicle battery reference capacity values.

	Min Capacity [kWh]	Med Capacity [kWh]	Max Capacity [kWh]
LCR	17.6	22	33
HCR	39.2	60	90
LCC	14.5	22.5	33
HCC	40	53	60

Table 9. Vehicle battery charge time.

	Min Capacity t_{ch} [h]	Med Capacity t_{ch} [h]	Max Capacity t_{ch} [h]
LCR	1.76	2.2	3.3
HCR	3.92	6	9
LCC	0.81	1.25	1.83
HCC	2.22	2.94	3.33

Table 10. Inerting time and time available for N2 production for EV categories.

	t_{in} [h]	Min Capacity t_{av} [h]	Med Capacity t_{av} [h]	Max Capacity t_{av} [h]
LCR	0.64	1.12	1.56	2.66
HCR	0.75	3.17	5.25	8.25
LCC	0.74	0.07	0.51	1.09
HCC	0.62	1.60	2.32	2.71

Table 11. Required N2 and produced N2 during grid operation.

	$n_{N_{2,inj}}$ [mol]	Min Capacity $n_{N_{2,grid}}$ [mol]	Med Capacity $n_{N_{2,grid}}$ [mol]	Max Capacity $n_{N_{2,grid}}$ [mol]
LCR	660.7	245.82	82.31	0
HCR	767.1	0	0	0
LCC	1367	1323.13	1025.84	635.65
HCC	1151.4	81.88	0	0

characterized by 0.093 m^2 and 0.35 m^2 area for the inlet and the outlet respectively. As example, Figure 4 depicts the obtained distribution of N_2 molar fraction in the box volume after 30 s and at the injection end, in the upper picture and in the lower one respectively.

The obtained spatial average value of the oxygen concentration within the protected volume (i.e. the $X_{O_{2,1}}$ parameter as previously indicated in Eqs. (6) and (10)) resulted in 11% after the N_2 injection for 60 s (lower picture of Figure 3). Moreover, the real injected N_2 amount provided the estimation of the *N* parameter equal to 1.2.

4. EV charge and grid power supply throud gh VAB

Box protection is performed by an ORS based on a VAB, reducing the oxygen concentration in the protected volume and at the same time charging the vehicle battery. In order to perform the energy analysis, vehicle battery capacity is assumed from values in Table 2 for each vehicle category; obtained reference values are shown in Table 8.

VAB power is set to 10 kW_e for LCR and HCR, and 18 kW_e for LCC and HCC, charge time for vehicle category is reassumed in Table 9.

Data from Table 4 and Eqs. (6), (7), (8), and (9) can be used to calculate inerting time, and charge time available to N_2 production (t_{av}) by Eq. (11).

$$t_{av} = t_{ch} - t_{in}\ [h] \tag{11}$$

Where t_{ch} is the vehicle charge time, and t_{in} is the inerting time obtained through Eqs. (6), (7), (8), and (9) converted in h (phase duration described at point 2 of the protection strategy). Calculated values are reassumed in Table 10.

The amount of N_2 moles which result during t_{av} up to the full vehicle charging ($n_{N_{2,prod}}$), can be calculated according to Eq. (12). In case this quantity is lower than the amount of N_2 to be injected in the protected volume, $n_{N_{2,inj}}$ is determined by Eq. (10), the VAB can continue its discharge towards local loads or the grid providing an additional N_2 production ($n_{N_{2,grid}}$ as determined by Eq. (13) see Table 11).

$$n_{N_{2,prod}} = Q_{O_{2,VAB}} \cdot \left(\frac{100 - X_{O_{2,std}}}{X_{O_{2,std}}}\right) \cdot t_{av} \cdot 3600\ [mol] \tag{12}$$

$$n_{N_{2,grid}} = n_{N_{2,inj}} - n_{N_{2,prod}}\ [mol] \tag{13}$$

The duration of this additional operation of the VAB providing energy to the grid or local loads (t_{grid}) can be calculated by Eq. (14).

$$t_{grid} = \left(\frac{n_{N_{2,grid}}}{Q_{O_{2,VAB}} \cdot 3600}\right) \cdot \left(\frac{X_{O_{2,std}}}{100 - X_{O_{2,std}}}\right)[h] \tag{14}$$

Calculated values for t_{grid} and relative energy to be supplied to the grid/utility are reassumed in Table 12.

Data in Table 12 for supplied energy show that the VAB can be operated simultaneously both for EV charge and box protection. Only for few vehicles, especially LCC, the VAB discharge must continue, suppling local stationary loads, after the EV full charge in order to restore the N_2 and to allow a subsequent EV charge. It is also highlighted that the N_2 amount to be restored is over-estimated since the gross volume of the protected internal environment is considered in the calculation. Battery capacity and the volume of vanadium anolyte solution to be stored to feed the anode section are reported in Table 13. The reported data are referred to anolyte energy and mass density of 50 Wh kg^{-1} and 1400 kg m^{-3} respectively [31], and a coulombic efficiency of 80% [25].

In addition to the described VAB fire protection function, domestic BESS utilization implies widely known benefits, such as increasing renewable self-consumption. A BESS is a fundamental element for peak-load reduction when EV charge must be provided, decoupling the distribution grid from demand load. In an increasing EV penetration scenario benefit of peak shaving can be found on the energy production side, reducing the utilization of low efficiency peak plants, on the transmission and distribution side, reducing the need of infrastructure upgrade, and on final users who can reduce energy expenditure shifting the demand in off-peak hours. High peak-shaving performances could be expected when storage battery capacity is over 20 kWh [32] with renewable energy systems integration. Grid services are also possible for behind-the-meter BESS, like voltage support, backup provision, frequency regulation and congestion and load leveling [33].

Table 12. VAB grid operation time and supplied energy.

	Min Capacity t_{grid} [h]	Med Capacity t_{grid} [h]	Max Capacity t_{grid} [h]	Min Capacity E_{grid} [kWh]	Med Capacity E_{grid} [kWh]	Max Capacity E_{grid} [kWh]
LCR	0.66	0.22	0	6.62	2.22	0
HCR	0	0	0	0	0	0
LCC	1.98	1.53	0.95	35.61	27.61	17.11
HCC	0.12	0	0	2.2	0	0

Table 13. VAB capacity and anolyte solution volume.

	Min Capacity C_{VAB} [kWh]	Med Capacity C_{VAB} [kWh]	Max Capacity C_{VAB} [kWh]	Min Capacity V_{an} [m^3]	Med Capacity V_{an} [m^3]	Max Capacity V_{an} [m^3]
LCR	24.22	24.22	33	0.43	0.43	0.59
HCR	39.2	60	90	0.70	1.07	1.61
LCC	50.11	50.11	50.11	0.89	0.89	0.89
HCC	42.2	53	60	0.75	0.95	1.07

5. Conclusions

VAB is a technology at early stage, the fire safety function can be considered a relevant added value if compared to other charging technologies. In this specific framework, the EV sector could be an interesting application, mostly for a lack of early warning systems against the thermal runaway. The fire protection concept of an ORS system is based on lowering the oxygen levels before the fire starts, then nitrogen generators are considered more convenient if compared with N_2 purchase. According to the economic evaluation performed in this work the VAB useful life must exceed 2.5 years in order to be competitive with N_2 purchase. A protection box could be built using established prefabricated technologies [34], evaluating fire performances [35] and airtightness [36] for the functional requirements of this specific application, a full development including nitrogen storage and injection system could be implemented in future works. Moreover, it is highlighted as the VAB utilization to charge EVs could limit the electric peak demand improving grid management performances and allow the exploitation of renewable electricity produced at the user side (with additional economic benefits), while providing the fire protection functionality. Considering that Li-ion batteries can be largely considered as the most used for EV and the growth of the EV market expected in the next future, the proposed system is supposed to have a growing impact during the next years.

Declarations

Author contribution statement

Barelli, L.: Conceived and designed the experiments; Analyzed and interpreted the data; Wrote the paper.

Bidini, G., Gallorini, F. & Serangeli, M: Analyzed and interpreted the data.

Ottaviano, P.A.: Analyzed and interpreted the data; Contributed reagents, materials, analysis tools or data.

Pelosi, D.: Conceived and designed the experiments; Performed the experiments; Wrote the paper.

Perla, M.: Analyzed and interpreted the data; Contributed reagents, materials, analysis tools or data; Wrote the paper.

Trombetti, L.: Contributed reagents, materials, analysis tools or data.

Funding statement

This research did not receive any specific grant from funding agencies in the public, commercial, or not-for-profit sectors.

Data availability statement

Data included in article/supp. material/referenced in article.

Declaration of interests statement

The authors declare no conflict of interest.

Additional information

No additional information is available for this paper.

References

[1] X. Feng, D. Ren, X. He, M. Ouyang, Mitigating thermal runaway of lithium-ion batteries, Joule 4 (2020) 743–770.
[2] X. Lai, S. Wang, H. Wang, Y. Zheng, X. Feng, Investigation of thermal runaway propagation characteristics of lithium-ion battery modules under different trigger modes, Int. J. Heat Mass Tran. 171 (2021) 121080.
[3] D. Ren, X. Feng, L. Liu, H. Hsu, L. Lu, L. Wang, X. He, M. Ouyang, Investigating the relationship between internal short circuit and thermal runaway of lithium-ion batteries under thermal abuse condition, Energy Storage Mater 34 (2021) 563–573.
[4] X. Feng, S. Zheng, D. Ren, X. He, L. Wang, X. Liu, M. Li, M. Ouyang, Key characteristics for thermal runaway of Li-ion batteries, Energy Procedia 158 (2019) 4684–4689.
[5] X. Feng, M. Fang, X. He, M. Ouyang, L. Lu, H. Wang, M. Zhang, Thermal runaway features of large format prismatic lithium ion battery using extended volume accelerating rate calorimetry, J. Power Sources 255 (2014) 294–301.
[6] S. Al Hallaj, H. Maleki, J.S. Hong, J.R. Selman, Thermal modeling and design considerations of lithium-ion batteries, J. Power Sources 83 (1999) 1–8.
[7] G. Guo, B. Long, B. Cheng, S. Zhou, P. Xu, B. Cao, Three-dimensional thermal finite element modeling of lithium-ion battery in thermal abuse application, J. Power Sources 195 (2010) 2393–2398.
[8] C. Qi, Y.L. Zhu, F. Gao, S.C. Wang, K. Yang, Q.J. Jiao, Safety analysis of lithium-ion battery by rheology-mutation theory coupling with fault tree method, J. Loss Prev. Process. Ind. 49 (2017) 603–611.
[9] S. Jamieson, Electric Car Gutted by Flames after it Set Fire while Charging, 2017. Telegr.
[10] P. Sun, R. Bisschop, H. Niu, X. Huang, A Review of Battery Fires in Electric Vehicles, 2020.
[11] J. Aelberts, Brandende Tesla Moet Nachtje in Bad Om Vlammen Te Doven, HLN, 2019.
[12] E. Huang, Electric Vans from One of China's Biggest EV Makers Are Catching Fire, Quartz, 2019.
[13] US Department of Transportation - Federal Aviation Administration, Extinguishment of Lithium-Ion and Lithium-Metal Battery Fires, 2017.
[14] P. Russo, C. Di Bari, M. Mazzaro, A. De Rosa, I. Morriello, Effective fire extinguishing systems for lithium-ion battery, Chem. Eng. Trans. 67 (2018) 727–732.
[15] R.T. Long Jr., A.F. Blum, T.J. Bress, B.R.T. Cotts, H.R.R.T. The, T. Observations, A. Fallis, Best practices for emergency response to incidents involving electric vehicles battery hazards: a report on full-scale testing results, J. Chem. Inf. Model. 53 (2013) 1009–1010.
[16] IEA, Global EV outlook, IEA, 2020. https://www.iea.org/reports/global-ev-outlook-2020. (Accessed 10 September 2020).
[17] N.E.F. Bloomberg, Electric vehicle outlook, Bloomberg Finance, 2020. https://about.bnef.com/electric-vehicle-outlook/. (Accessed 7 September 2020).
[18] M. Woodward, B. Walton, J. Hamilton, Electric vehicles - setting a course for 2030, Deloitte insights, https://www2.deloitte.com/us/en/insights/focus/future-of-mobility/electric-vehicle-trends-2030.html (accessed December 7, 2020).
[19] T&E (Transport & Environment), Electric Surge: Carmakers' Electric Car Plans across Europe 2019-2025, 2019.
[20] UNRAE - unione nazionale rappresentanti autoveicoli esteri, UNRAE, http://www.unrae.it/ (accessed April 23, 2020).
[21] European Committee for Standardization, Fixed Firefighting Systems - Oxygen Reduction Systems - Design, Installation, Planning and Maintenance EN 16750, 2017.
[22] P. Berg, A. Lindgren, Fire Prevention and Health Assessment in Hypoxic Environment, 2004.
[23] A.W. Golubkov, D. Fuchs, J. Wagner, H. Wiltsche, C. Stangl, G. Fauler, G. Voitic, A. Thaler, V. Hacker, Thermal-runaway experiments on consumer Li-ion batteries with metal-oxide and olivin-type cathodes, RSC Adv. 4 (2014) 3633–3642.
[24] I.A. Zlochower, G.M. Green, The limiting oxygen concentration and flammability limits of gases and gas mixtures, J. Loss Prev. Process. Ind. 22 (2009) 499–505.
[25] J.G. Austing, C.N. Kirchner, E.M. Hammer, L. Komsiyska, G. Wittstock, Study of an unitised bidirectional vanadium/air redox flow battery comprising a two-layered cathode, J. Power Sources 273 (2015) 1163–1170.
[26] E. Sánchez-Díez, E. Ventosa, M. Guarnieri, A. Trovò, C. Flox, R. Marcilla, F. Soavi, P. Mazur, E. Aranzabe, R. Ferret, Redox flow batteries: status and perspective towards sustainable stationary energy storage, J. Power Sources 481 (2021).
[27] X. Han, X. Li, J. White, C. Zhong, Y. Deng, W. Hu, T. Ma, Metal–air batteries: from static to flow system, Adv. Energy Mater. 8 (2018) 1–28.
[28] W. Huang, X. Feng, X. Han, W. Zhang, F. Jiang, Questions and answers relating to lithium-ion battery safety issues, Cell Reports Phys. Sci. 2 (2021) 100285.

[29] J.G. Austing, C.N. Kirchner, L. Komsiyska, G. Wittstock, Layer-by-layer modification of Nafion membranes for increased life-time and efficiency of vanadium/air redox flow batteries, J. Membr. Sci. 510 (2016) 259–269.
[30] J. Noack, C. Cremers, D. Bayer, J. Tübke, K. Pinkwart, Development and characterization of a 280 cm2 vanadium/oxygen fuel cell, J. Power Sources 253 (2014) 397–403.
[31] F. Moro, A. Trovò, S. Bortolin, D. Del Col, M. Guarnieri, An alternative low-loss stack topology for vanadium redox flow battery: comparative assessment, J. Power Sources 340 (2017) 229–241.
[32] K. Mahmud, S. Member, M.J. Hossain, S. Member, Peak-Load Management in Commercial Systems with Electric Vehicles, 2018, pp. 1–11.
[33] C. Jankowiak, A. Zacharopoulos, C. Brandoni, P. Keatley, P. Macartain, N. Hewitt, The Role of Domestic Integrated Battery Energy Performance Enhancement, 2019, pp. 1–27.
[34] M.K. Faidzi, S. Abdullah, M.F. Abdullah, A.H. Azman, D. Hui, S.S.K. Singh, Review of current trends for metal-based sandwich panel: failure mechanisms and their contribution factors, Eng. Fail. Anal. 123 (2021) 105302.
[35] R.J. Crewe, J.P. Hidalgo, M.X. Sørensen, M. McLaggan, S. Molyneux, S. Welch, G. Jomaas, J.L. Torero, A.A. Stec, T.R. Hull, Fire performance of sandwich panels in a modified ISO 13784-1 small room test: the influence of increased fire load for different insulation materials, Fire Technol. 54 (2018) 819–852.
[36] K. Orlowski, K. Shanaka, P. Mendis, Design and Development of weatherproof seals for prefabricated construction: a methodological approach, Buildings 8 (2018).